On the Interplay Between Electrical Conductivity and Seebeck Coefficient in Ultra-Narrow Silicon Nanowires

Neophytos Neophytou & Hans Kosina

Journal of Electronic Materials

ISSN 0361-5235

Journal of Elec Materi
DOI 10.1007/s11664-011-1891-7

Springer

Journal of ELECTRONIC MATERIALS
DOI: 10.1007/s11664-011-1891-7

On the Interplay Between Electrical Conductivity and Seebeck Coefficient in Ultra-Narrow Silicon Nanowires

NEOPHYTOS NEOPHYTOU[1,2] and HANS KOSINA[1,3]

1.—Institute for Microelectronics, TU Wien, Gußhausstraße 27-29/E360, A-1040 Wien, Austria. 2.—e-mail: neophytou@iue.tuwien.ac.at. 3.—e-mail: kosina@iue.tuwien.ac.at

We analyze the effect of low dimensionality on the electrical conductivity (σ) and Seebeck coefficient (S) in ultra-narrow Si nanowires (NWs) by employing atomistic considerations for the electronic structures and linearized Boltzmann transport theory. We show that changes in the geometrical features of the NWs such as diameter and orientation mostly affect σ and S in two ways: (i) the distance of the band edges from the Fermi level (η_F) changes, and (ii) quantum confinement in some cases strongly affects the effective mass of the subbands, which influences the conductivity of the NWs and η_F. Changes in η_F cause exponential changes in σ but linear changes in S. S seems to be only weakly dependent on the curvature of the bands, the strength of the scattering mechanisms, and the shape of the density of states function DOS(E), contrary to current view. Our results indicate that low dimensionality has a stronger influence on σ than on S due to the greater sensitivity of σ to η_F. We identify cases where bandstructure engineering through confinement can improve σ without significantly affecting S, which can result in power factor improvements.

Key words: Thermoelectric, electrical conductivity, Seebeck coefficient, tight binding, atomistic, $sp^3d^5s^*$, Boltzmann transport, silicon, nanowire

INTRODUCTION

The ability of a material to convert heat into electricity is measured by the dimensionless figure of merit $ZT = \sigma S^2 T/(\kappa_e + \kappa_l)$, where σ is the electrical conductivity, S is the Seebeck coefficient, and κ_e and κ_l are the electronic and lattice parts of the thermal conductivity, respectively. Some of the best thermoelectric materials are based on rare-earth or toxic elements and exhibit $ZT \approx 1$. Recent breakthrough experiments on nanostructured thermoelectrics, however, have demonstrated that κ_l can be significantly suppressed, offering large improvements in ZT compared with the raw materials' values. Such effects have been observed for one-dimensional (1D) nanowires (NWs),[1,2] two-dimensional (2D) thin films, 1D/2D superlattices,[3,4] as well as materials with embedded nanostructuring.[5] More importantly, this has been achieved for common materials such as Si, SiGe, and InGaAs. In silicon, although the bulk material has $ZT_{bulk} \approx 0.01$, the ZT of silicon NWs with side lengths scaled down to 10–50 nm was experimentally demonstrated to be $ZT_{NW} \approx 0.5$.[1,2]

On the other hand, it has been suggested by Hicks and Dresselhaus[6] that low dimensionality can be beneficial to the power factor σS^2 as well. The sharp features in the low-dimensional density of states, DOS(E), can improve S, as this quantity is proportional to the energy derivative of DOS(E).[7] This was actually the initial drive towards low-dimensional thermoelectrics. Although S and σ are inversely proportional, it was suggested that low-dimensional DOS(E) could potentially improve S without reducing σ. This effect, however, has not yet been experimentally confirmed because the sharp features in DOS(E) disappear in the presence of nonidealities.

(Received July 15, 2011; accepted December 22, 2011)

Published online: 01 February 2012

In this work, we discuss the influence of low dimensionality on the Seebeck coefficient, and the interplay between the Seebeck coefficient and the electrical conductivity in ultra-narrow NWs of diameters below $D = 12$ nm. We couple the 20 orbital atomistic $sp^3d^5s^*$ spin–orbit-coupled (SO) tight-binding (TB) model[8] to linearized Boltzmann transport theory.[9–11] Our analysis shows that low dimensionality affects the electronic conductivity more strongly than the Seebeck coefficient. The Seebeck coefficient is weakly dependent on the curvature of the bands, the strength of the scattering mechanisms, and even the shape of the DOS(E) function. It is mostly dependent on the distance of the subband edges from the Fermi level (η_F). This dependence of S on η_F is close to linear, but the dependence of σ on η_F is exponential. We then indicate bandstructure engineering cases for which σ is improved with quantum confinement without significant reductions in S, situations which can result in power factor improvements.

APPROACH

The $sp^3d^5s^*$ SO tight-binding model[8] accurately captures the electronic structures and inherently includes the effects of quantum confinement. It represents a compromise between computationally expensive fully *ab initio* methods and numerically inexpensive but less accurate effective-mass models. Our calculations can include up to 5500 atoms, a challenging but achievable computational task within this model. We consider infinitely long, cylindrical NWs with hydrogen-passivated surfaces.[12] No lattice relaxation is assumed for the NW surfaces.

The electrical conductivity and Seebeck coefficient follow from linearized Boltzmann theory as

$$\sigma = q_0^2 \int_{E_0}^{\infty} dE \left(-\frac{\partial f_0}{\partial E}\right) \Xi(E), \tag{1a}$$

$$S = \frac{q_0 k_B}{\sigma} \int_{E_0}^{\infty} dE \left(-\frac{\partial f_0}{\partial E}\right) \Xi(E) \left(\frac{E - E_F}{k_B T}\right), \tag{1b}$$

where the transport distribution function $\Xi(E)$ is defined as[13,14]

$$\begin{aligned} \Xi(E) &= \sum_{k_x,n} v_n^2(k_x)\tau_n(k_x)\delta(E - E_n(k_x)) \\ &= \sum_n v_n^2(E)\tau_n(E) g_{1D}^n(E), \end{aligned} \tag{2}$$

where $v_n(E) = \partial E_n/\hbar\partial k_x$ is the bandstructure velocity, $g_{1D}^n(E) = 1/(2\pi\hbar v_n(E))$ is the density of states for the 1D subbands (per spin), and $\tau_n(k_x)$ is the momentum relaxation time for a state with k_x in subband n. For this calculation we use the velocity $v_i(k_x)$ instead of the momentum k_x in the definition of the relaxation time as

$$\frac{1}{\tau_n(k_x)} = \sum_{m,k_x'} S_{n,m}\left(k_x, k_x'\right)\left(1 - \frac{v_m(k_x')}{v_n(k_x)}\right). \tag{3}$$

The two are equivalent for parabolic bands, and both are valid approximations resulting from more complicated integral equations as described in Refs. 15,16. The transition rate $S_{n,m}(k_x, k_x')$ for a carrier in an initial state k_x in subband n to a final state k_x' in subband m is extracted from the electronic dispersions and the atomistically extracted wave form overlaps using Fermi's Golden Rule. The entire procedure is described in detail in Ref. 14.

We include phonon and surface roughness scattering (SRS). For phonon scattering we include all relevant mechanisms of bulk silicon.[17] Although we still employ bulk phonons, this should not affect our conclusions significantly, as discussed in Refs. 9,11,18. All deformation potential values and phonon energies used are from Ref. 17 with the exceptions of $D_{ODP}^{hole} = 13.24 \times 10^{10}$ eV/m, $D_{ADP}^{hole} = 5.34$ eV, and $D_{ADP}^{electron} = 9.5$ eV from Refs. 9,11,18, which are more relevant for NWs.

For SRS we assume a 1D exponential autocorrelation function[19] for the roughness with $\Delta_{rms} = 0.48$ nm and $L_C = 1.3$ nm.[20] The momentum relaxation rate is derived from the shift in the band edges with quantization, as described by Uchida and Takagi[21] and Fang et al.[22] as

$$\frac{1}{\tau_{SRS}^n} = \frac{2\pi}{\hbar}\left(\frac{2\Delta_{rms}^2 L_C}{1 + q^2 L_C^2}\right)\left(\frac{q_0 \Delta E_0}{\Delta D}\right)^2 \sum_m g_{1D}^m(E), \tag{4}$$

where $q = k_x - k_x'$. As discussed in Ref. 21, this is a valid approach for describing SRS in ultra-thin channels of a few nanometers in thickness.

RESULTS AND DISCUSSION

To illustrate the diameter dependence of electrical conductivity and Seebeck coefficient, Fig. 1 shows these quantities for the n-type [100]-oriented NW versus diameter for carrier concentration $n = 10^{19}/cm^3$ (close to where the peak of the power factor appears[23]). The dashed lines indicate the phonon-limited results, whereas the solid lines include phonons and SRS. Figure 1a shows the electrical conductivity. Comparing at the same carrier concentration, the conductivity is degraded by ~4× as the diameter is reduced. The effect of SRS causes an additional ~2× degradation (for the lower diameters). This degradation does not appear in the case of ballistic transport where the ballistic conductance G (normalized by the NW's area in nm^2) is almost unchanged as the diameter is reduced (inset of Fig. 1a).[24]

The Seebeck coefficient in Fig. 1b increases as the diameter is reduced, especially for diameters below

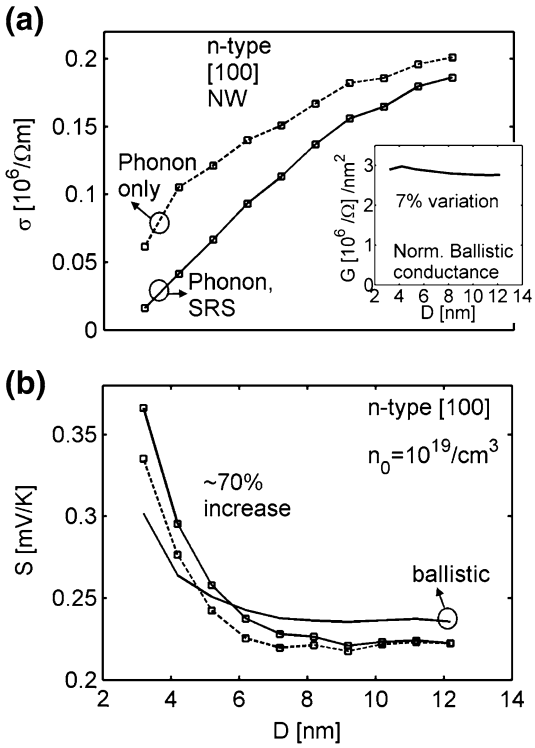

Fig. 1. Electrical conductivity (a) and Seebeck coefficient (b) for *n*-type NWs in the [100] transport orientation at $n = 10^{19}/\text{cm}^3$ versus diameter. Dashed lines with squares: Only phonon scattering is considered. Solid lines with squares: Phonons and SRS are considered. Solid lines: Ballistic conditions. Inset of (a) shows the ballistic conductance per unit area (normalized by the nanowire area in nm^2) versus diameter.

$D = 7$ nm, following the inverse trend compared with conductivity, since these quantities are inversely proportional. The increase is ~70% and can be observed under scattering as well as ballistic conditions (smaller for ballistic). Including SRS causes only a slight additional increase from the phonon-limited result and ballistic results, indicating that S is to first order independent of scattering.

The explanation for these trends originates from the placement of the subband edges in energy with respect to the Fermi level for each NW. The carrier concentration is given by

$$n_{3D} = \frac{M}{A}\int_{E_0} g_{1D}(E) f(E - E_F)\mathrm{d}E, \qquad (5)$$

where M is the number of subbands, A is the normalization cross-section area, and E_F is the Fermi level. As the area is reduced, the number of subbands M decreases, usually linearly for the thicker NWs such that the ratio M/A remains constant. At some point, only a few or even only one subband participates in transport. Usually for Si at room temperature this happens at $D < 10$ nm. Further reduction of the NW area will not be linearly compensated by reduction in M, and the ratio M/A will increase following $\sim 1/A$ as M approaches closer to 1.

To keep the carrier concentration n_{3D} constant, the energy integral has to be reduced, which is achieved when the distance of the subband edges E_0 from the Fermi level $\eta_F = E_0 - E_F$ is increased. This is demonstrated in Fig. 2, which compares the position of the Fermi level for n-type [100] NWs with $D = 12$ nm and $D = 3$ nm at the same carrier concentration. Figure 2a and b show the dispersion relations for the two NWs, respectively, for $n = 10^{19}/\text{cm}^3$. The dispersions are shifted to $E_0 = 0$ eV, and the position of the Fermi level is indicated. η_F is larger for the $D = 3$ nm NW. Figure 2c shows η_F for the two NWs versus carrier concentration. At carrier concentrations from $10^{18}/\text{cm}^3$ to $10^{20}/\text{cm}^3$, where the power factor in Si is the highest, the difference in η_F between the two NWs is ~40 meV. It is also important to note the dependence of the shift of η_F on changes of the ratio M/A. Using $g^n_{1D}(E) \propto \sqrt{m_{\text{eff}}/\tilde{E}}$ (valid for 1D and parabolic bands), where $\tilde{E} = E - E_0$, and m_{eff} is the effective mass of the subband,

$$n_{3D} = m_{\text{eff}}\left(\frac{M}{A}\right)\int_{E_0}^{\infty} \tilde{E}^{-1/2} f(E - E_F)\mathrm{d}E. \qquad (6)$$

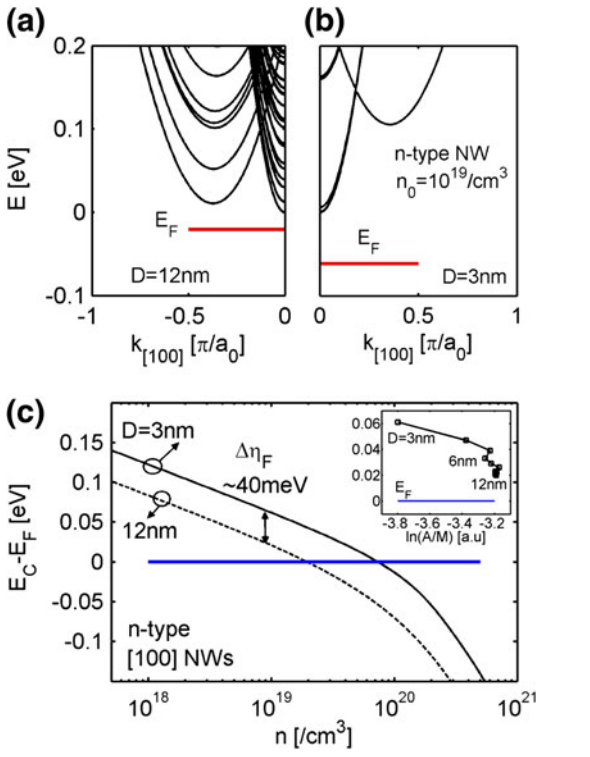

Fig. 2. Electronic structures for *n*-type [100] NWs: (a) $D = 12$ nm, and (b) $D = 3$ nm. The position of the Fermi level for carrier concentrations $n = 10^{19}/\text{cm}^3$ is shown for each case. (c) The difference of the dispersion band edges from the Fermi level (η_F) for NWs with $D = 12$ nm (dashed) and $D = 3$ nm (solid) versus the carrier concentration. Inset of (c) shows η_F versus $\ln(A/M)$, where A is the NW area. For M we use the density of states up to 0.2 eV from the edge of the conduction band edge.

The energy integral is an exponential function of η_F through the Fermi distribution (under non-degenerate conditions, for $\eta_F > 0$). In order to keep the same carrier concentration under changes in M/A (assuming constant m_{eff}), η_F changes, but it needs to do so only *logarithmically*. From Eq. 6, therefore, one can observe that, to first order, $\Delta\eta_F \propto \ln(M/A)$. The inset of Fig. 2c shows $\eta_F = E_C - E_F$ versus $\ln(A/M)$. We have flipped the numerator and denominator to have the narrowest NWs to the left. Here, for M we use the density of states below a cutoff energy of 0.2 eV above the conduction band edge. For larger diameters, A/M and $\ln(A/M)$ are almost constant (right side of inset), and η_F shifts little. Most of the change in $\ln(A/M)$ and η_F comes at lower diameters, as expected, where η_F follows a more or less linear trend.

When η_F increases, the conductivity decreases. For a rough qualitative understanding of how the conductivity is affected, we substitute Eq. 2 into Eq. 1a. We assume that $\tau_n(E)$ follows a simple relation (at least for elastic isotropic processes, such as acoustic phonon scattering) as

$$\tau_n(E) \propto \frac{A}{M g_{1D}^n(E)}, \tag{7}$$

which just means that the scattering rates are proportional to the density of states into which a carrier can scatter. Now we substitute these relations into Eq. 1a to obtain (after performing the summation over the subbands in Eq. 2)

$$\sigma \propto \int_{E_0} v_n^2(E) \frac{A}{M g_{1D}^n(E)} \frac{M g_{1D}^n(E)}{A} \left(-\frac{\partial f(E-E_F)}{\partial E}\right) dE = \int_{E_0} v_n^2(E) \left(-\frac{\partial f(E-E_F)}{\partial E}\right) dE. \tag{8}$$

Using $g_{1D}^n(E) \propto \sqrt{m_{eff}/\tilde{E}}$ and $v_n(E) \propto \sqrt{\tilde{E}/m_{eff}}$, then

$$\sigma \propto \int_{E_0}^{\infty} \tilde{E}/m_{eff} \left(-\frac{\partial f(E-E_F)}{\partial E}\right) dE = \frac{1}{m_{eff}} \tilde{F}(\eta_F), \tag{9}$$

where $\tilde{F}(\eta_F)$ is a function of η_F, independent of band structure to first order, and exponentially decreasing with increasing η_F (again under non-degenerate conditions, for $\eta_F > 0$). As described earlier, when the NW area is reduced, the ratio M/A increases, forcing η_F to also increase logarithmically (as M approaches to 1) in order to keep a constant carrier concentration. This results in a $\sim 1/A$ decrease in the function $\tilde{F}(\eta_F)$ ($\Delta\tilde{F}(\eta_F)$) with cross-section area scaling. Following the $\tilde{F}(\eta_F)$ trend, the conductivity decrease ($\Delta\sigma$) also follows $\sim 1/A$ to first order (or $1/D^2$ as indicated in the phonon-limited results in Fig. 1a).

Similarly, the Seebeck coefficient can be shown to follow

$$S \propto \frac{\int_{E_0}^{\infty} F(\eta_F)\left(\frac{E-E_F}{k_B T}\right) dE}{\int_{E_0}^{\infty} F(\eta_F) dE}, \tag{10}$$

where $F(\eta_F) = \tilde{E}\left(-\frac{\partial f(E-E_F)}{\partial E}\right)$. The Seebeck coefficient is therefore first order independent of band structure, and reduces linearly as the energy deviates from the Fermi level as expected [$F(\eta_F)$ is found in both numerator and denominator]. As shown in Fig. 1b, at larger NW diameters where η_F is small and does not vary significantly, S is constant. As the NW diameter is reduced and η_F increases logarithmically, S also increases logarithmically. The magnitude of this logarithmic increase in S with A (or D) scaling, however, is smaller compared with the magnitude of the decrease in σ, which follows $1/A$ (or $1/D^2$).

It is important, however, to stress that the trend presented in Fig. 1 is at constant carrier concentration. Alternatively, the diameter behavior can be presented in terms of constant η_F. Figure 3 shows the phonon-limited electrical conductivity and Seebeck coefficient versus the NW diameter for the cases: (i) constant carrier concentration (same as in Fig. 1), and (ii) constant $\eta_F = k_B T$. The behavior under constant η_F is different. The electrical conductivity (Fig. 3a) is almost constant (also indicated from Eq. 9), with a slight increase as the diameter is reduced because of the reduction in the available subbands and states into which the carriers can scatter. The Seebeck coefficient (Fig. 3b) is also almost constant with diameter, as can be understood from Eq. 10. This is an interesting observation, which shows that it is the distance of the band edges from the Fermi level that controls S, whereas the shape of DOS(E) does not affect S significantly. Indeed, DOS(E) for the D = 3 nm NW shows 1D-like behavior, whereas that of the D = 12 nm NW is different, with many more closely packed subband peaks. This is in agreement with the results by Kim et al.[25] for 1D, 2D, and three-dimensional (3D) channels. However, no matter how one presents the diameter dependence, at either constant concentration or constant η_F, the effect of reducing the diameter from D = 12 nm (almost bulk-like) to D = 3 nm (1D), does not improve the power factor significantly, as shown in Fig. 3c. There is only a moderate improvement for smaller diameters if η_F is held constant as the diameter is reduced.

There are situations, however, where the effective mass of the subbands reduces as the NW diameter is reduced. As we have shown in our previous works, this is the case for p-type [110] and [111] NWs,[11,26] and to a smaller degree for n-type [110] NWs.[27] This is shown in Fig. 4a and b for the p-type [110] D = 12 nm and D = 3 nm NWs, respectively. The curvature of the subbands of the D = 3 nm NW is

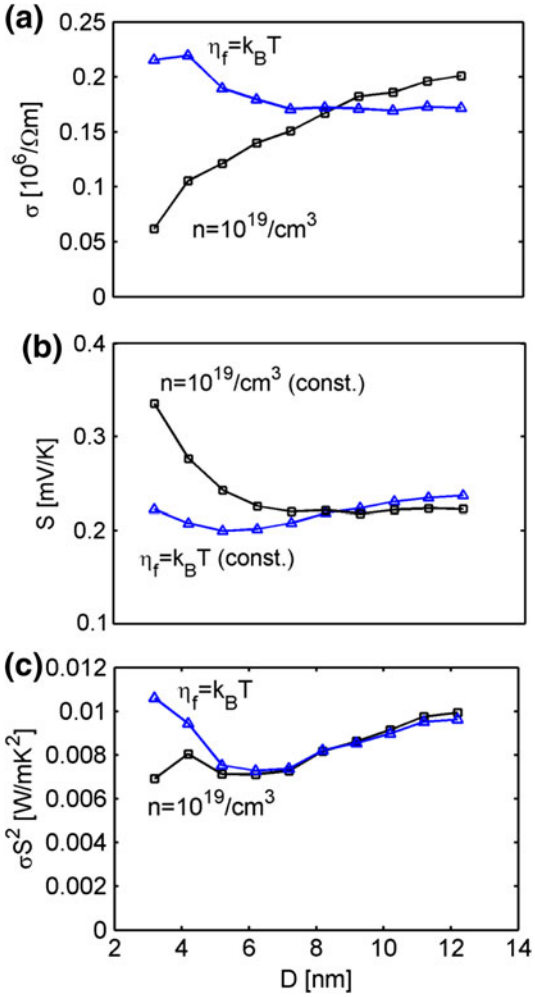

Fig. 3. Thermoelectric coefficients for *n*-type NWs in [100] transport orientation versus diameter. Two conditions are shown: (i) constant carrier concentration $n = 10^{19}/\text{cm}^3$ (black lines with squares), and (ii) constant $\eta_F = k_B T$ (blue lines with triangles). (a) Electrical conductivity. (b) Seebeck coefficient. (c) Power factor.

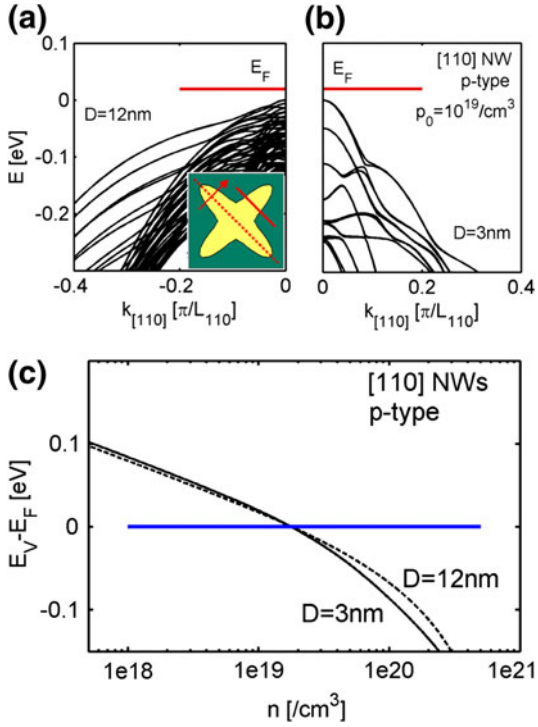

Fig. 4. Electronic structures for *p*-type [110] NWs: (a) $D = 12$ nm, and (b) $D = 3$ nm. The position of the Fermi level for carrier concentrations $p = 10^{19}/\text{cm}^3$ is shown for each case. (c) The difference of the dispersion band edges from the Fermi level (η_F) for the NWs with $D = 12$ nm (dashed) and $D = 3$ nm (solid) versus the carrier concentration. Inset of (a) shows a schematic of the heavy-hole band of bulk Si. The dotted line indicates the relevant bulk energy bands. Confinement shifts the relevant bands in the direction of the arrow towards the solid line.

larger than for $D = 12$ nm, indicating a smaller m_{eff} and DOS compared with the $D = 12$ nm NW. The reason behind the effective mass reduction with diameter scaling is related to the strongly anisotropic warped shape of the heavy-hole valence band as shown in the inset of Fig. 4a. For bulk materials, the effective mass is determined by the curvature of the $E(k)$ relation along the dashed line passing though the center of the Brillouin zone. Upon confinement, the low-dimensional subbands are formed from energy subbands away from the center (direction of the arrow) as indicated by the solid line in the inset of Fig. 4a, similar to the "particle in a box" quantization picture. Since the heavy-hole is highly anisotropic, the curvature of the bands increases significantly, and the effective mass is reduced. We note that the lines shown represent confinement along the (110) surface and transport along the [110] orientation, which are the relevant orientations for the [110] NW. In the case of *n*-type NWs, because the conduction band is mostly isotropic along a specific direction, much smaller mass variations are observed.[27]

For the *p*-type [110] case, η_F will not increase with diameter scaling, in contrast to the *n*-type [100] NWs in Fig. 2a, b. The Fermi level calculated for carrier concentration $p = 10^{19}/\text{cm}^3$ is almost at the same position for both NWs. Figure 4c shows that η_F is almost the same for both NWs for a large range of carrier concentrations, except at very high ones. This is a result of two counteracting mechanisms: (i) as the diameter is reduced, η_F tends to increase, but (ii) as the effective mass reduces, in order to maintain the same carrier concentration, η_F is reduced again. These two counteracting effects finally leave η_F almost unchanged. In other words, the increase in M/A in Eq. 6 is compensated by the reduction in m_{eff}, and η_F remains unchanged. The trend of the conductivity and the Seebeck coefficient as a function of diameter will therefore be the same, at either constant concentration or constant η_F.

Figure 5 shows σ and S for *p*-type [110] NWs as a function of NW diameter at constant carrier concentration of $p = 10^{19}/\text{cm}^3$. In all cases, η_F is very similar, $\eta_F = 0.018 \pm 0.001$ eV. Phonon-limited

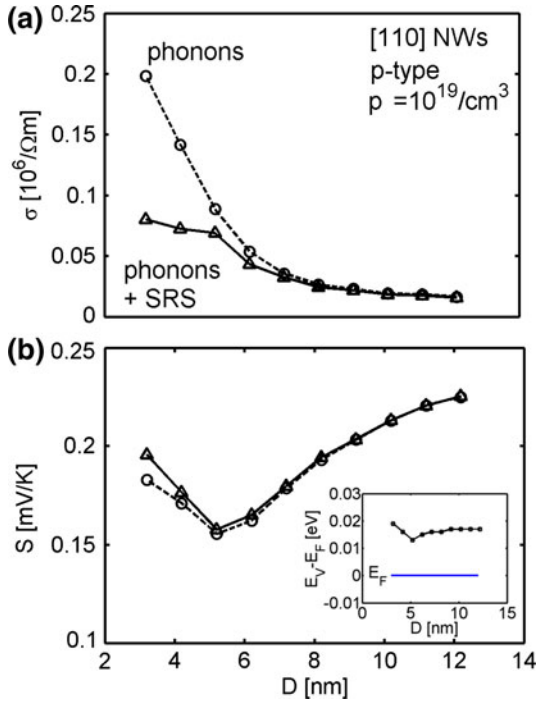

Fig. 5. Thermoelectric coefficients for *p*-type NWs in the [110] transport orientation versus diameter at carrier concentration $p = 10^{19}/cm^3$. Two conditions are shown: (i) phonon-limited results (dashed line with circles), and (ii) phonon- plus SRS-limited results (solid line with squares). (a) Electrical conductivity. (b) Seebeck coefficient. Inset of (b) shows η_F versus diameter.

(dashed lines with circles) and phonon- plus SRS-limited (solid line with triangles) results are shown. The electrical conductivity in Fig. 5a increases as the diameter is reduced, because the effective mass of the subbands decreases.[11] As indicated in Eq. 9, at constant η_F the only contribution to σ is from m_{eff}. SRS degrades the conductivity for the small-diameter NWs, but in this case the improvement due to the reduction in m_{eff} is large enough to compensate for this detrimental effect. On the other hand, the Seebeck coefficient in Fig. 5b does not change significantly with diameter since η_F is constant, as can also be deduced from Eq. 10. This results in a slightly reducing trend for most of the diameter range, a reverse trend compared with σ. At diameters below $D = 5$ nm, some increase is observed, which is again a result of the trend of η_F as shown in the inset of Fig. 5b. Another important observation is that the introduction of SRS in the calculation only slightly affects S. Unlike σ, S to first order only depends on η_F and not on the bandstructure; therefore, the introduction of more scattering mechanisms does not have a significant influence on it. The large increase in σ and the almost invariant S diameter trend in this *p*-type [110] NW case allow for improvements in the power factor of the channel.

CONCLUSIONS

The interplay between the electrical conductivity (σ) and the Seebeck coefficient (S) in narrow Si NWs of diameters below 12 nm is investigated. The $sp^3d^5s^*$ atomistic tight-binding model and linearized Boltzmann theory are employed. We show that, for a specific carrier concentration, as the diameter of the NWs is reduced, the band edges shift further with respect to the Fermi level (η_F increases) to first order logarithmically as a function of the NW's cross-section area. An increase in η_F reduces σ exponentially and increases S linearly. Due to the exponential dependence, σ is the quantity with the greatest influence on the power factor of NWs. As a function of diameter, the logarithmic increase of η_F to first order decreases σ as D^2 and increases S logarithmically. The curvature of the bands, the strength of the scattering mechanisms, and the shape of the DOS(E) function do not seem to affect S significantly as the diameter changes from $D = 3$ nm to $D = 12$ nm, in agreement with other reports.[25] We show that, in cases where the effective mass of the dispersion becomes lighter with confinement (i.e., *p*-type [110] NWs), η_F is less susceptible to NW diameter changes. In such case σ increases because of the m_{eff} reduction, whereas S changes only slightly because η_F changes only slightly, enabling improvements in the power factor.

ACKNOWLEDGEMENT

This work was supported by the Austrian Climate and Energy Fund, Contract No. 825467.

REFERENCES

1. A.I. Hochbaum, R. Chen, R.D. Delgado, W. Liang, E.C. Garnett, M. Najarian, A. Majumdar, and P. Yang, *Nature* 451, 163 (2008).
2. A.I. Boukai, Y. Bunimovich, J.T. Kheli, J.-K. Yu, W.A. Goddard III, and J.R. Heath, *Nature* 451, 168 (2008).
3. R. Venkatasubramanian, E. Siivola, T. Colpitts, and B.O. Quinn, *Nature* 413, 597 (2001).
4. W. Kim, S.L. Singer, A. Majumdar, D. Vashaee, Z. Bian, A. Shakouri, G. Zeng, J.E. Bowers, J.M.O. Zide, and A.C. Gossard, *Appl. Phys. Lett.* 88, 242107 (2006).
5. J. Tang, H.-T. Wang, D.H. Lee, M. Fardy, Z. Huo, T.P. Russell, and P. Yang, *Nano Lett.* 10, 4279 (2010).
6. L.D. Hicks and M.S. Dresselhaus, *Phys. Rev. B* 47, 16631 (1993).
7. J.P. Heremans, V. Jovovic, E.S. Toberer, A. Samarat, K. Kurosaki, A. Charoenphakdee, S. Yamanaka, and G.J. Snyder, *Science* 321, 554 (2008).
8. T.B. Boykin, G. Klimeck, and F. Oyafuso, *Phys. Rev. B* 69, 115201 (2004).
9. A.K. Buin, A. Verma, A. Svizhenko, and M.P. Anantram, *Nano Lett.* 8, 760 (2008).
10. V.M. Fomin and P. Kratzer, *Phys. Rev. B* 82, 045318 (2010).
11. N. Neophytou and H. Kosina, *Nano Lett.* 10, 4913 (2010).
12. S. Lee, F. Oyafuso, P. Von Allmen, and G. Klimeck, *Phys. Rev. B* 69, 045316 (2004).
13. T.J. Scheidemantel, C.A. Draxl, T. Thonhauser, J.V. Badding, and J.O. Sofo, *Phys. Rev. B* 68, 125210 (2003).
14. N. Neophytou and H. Kosina, *Phys. Rev. B* 83, 245305 (2011).

15. M.V. Fischetti, *J. Appl. Phys.* 89, 1232 (2001).
16. M.V. Fischetti, Z. Ren, P.M. Solomon, M. Yang, and K. Rim, *J. Appl. Phys.* 94, 1079 (2003).
17. M. Lundstrom, *Fundamentals of Carrier Transport* (Cambridge: Cambridge University Press, 2000).
18. A.K. Buin, A. Verma, and M.P. Anantram, *J. Appl. Phys.* 104, 053716 (2008).
19. S.M. Goodnick, D.K. Ferry, C.W. Wilmsen, Z. Liliental, D. Fathy, and O.L. Krivanek, *Phys. Rev. B* 32, 8171 (1985).
20. S. Jin, M.V. Fischetti, and T. Tang, *J. Appl. Phys.* 102, 83715 (2007).
21. K. Uchida and S. Takagi, *Appl. Phys. Lett.* 82, 2916 (2003).
22. T. Fang, A. Konar, H. Xing, and D. Jena, *Phys. Rev. B* 78, 205403 (2008).
23. N. Neophytou, H. Kosina, and J. Electr, *Materials* 40, 753 (2011).
24. N. Neophytou, M. Wagner, H. Kosina, S. Selberherr, and J. Electr, *Materials* 39, 1902 (2010).
25. R. Kim, S. Datta, and M.S. Lundstrom, *J. Appl. Phys.* 105, 034506 (2009).
26. N. Neophytou, S.G. Kim, G. Klimeck, and H. Kosina, *J. Appl. Phys.* 107, 113701 (2010).
27. N. Neophytou, A. Paul, M.S. Lundstrom, and G. Klimeck, *IEEE Trans. Electron. Dev.* 55, 1286 (2008).